Iranian Journal of Astronomy and Astrophysics
Vol. 12, No. 4, Autumn 2025, 299–310
©Available online at http://ijaa.du.ac.ir
DOI: 10.22128/ijaa.2026.3168.1234
Online ISSN: 2383–403X

Iranian Journal of Astronomy and Astrophysics

Research Paper

Criticality in Nonconformal Plasmas at Finite Temperature and Density

Leila Shahkarami
School of Physics, Damghan University, Damghan 36716-45667, Iran;
E-mail: l.shahkarami@du.ac.ir

Received: 28 November 2025; **Accepted:** 15 February 2026; **Published:** 16 February 2026

Abstract. We study the thermodynamics of an asymptotically AdS black hole in a holographic Einstein-Maxwell-dilaton model describing a nonconformal plasma at finite temperature and chemical potential. Using a logarithmic warp factor and working in the grand canonical ensemble, we analyze the temperature-horizon relation, entropy density, grand potential, pressure, energy density, and trace anomaly, demonstrating the emergence of a first-order phase transition at low chemical potentials, a critical end point, and a smooth crossover at higher chemical potentials. Thermodynamic response functions, including the heat capacity and charge susceptibility, exhibit finite jumps at the first-order transition, divergence at the critical end point, and broad maxima in the crossover region. These results collectively establish a consistent and QCD-like phase structure in this holographic framework.

Keywords: Dynamical Holographic QCD Model, Critical Behaviour.

1 Introduction

The study of strongly-coupled gauge theories at finite temperature and chemical potential remains a central challenge in theoretical physics. Among the frameworks developed to address this challenge, gauge/gravity duality (also known as holography) [1–4] offers a powerful tool, enabling insight into non-perturbative phenomena of QCD-like theories. In bottom-up constructions of holographic QCD, one often encounters limitations: for example, many confining phases in simplified models are insensitive to temperature or chemical potential, which restricts the possibility to explore the full phase diagram including finite-density effects.

In this framework, some of Einstein-Maxwell-Dilaton (EMD) models such as that proposed by Dudal and Mahapatra serve as a convenient phenomenological setup [5]. Confinement that depends on temperature and chemical potential can be realised only in bottom-up constructions that solve the Einstein equations from a well-defined gravitational action. In its version with a logarithmic warp-factor ansatz, the model allows for a finite-temperature confining branch (realized by a small black hole rather than thermal AdS) and produces a rich phase structure: a first-order line at low chemical potential terminating at a critical end point (CEP), and a supercritical region beyond it. This feature makes the model particularly suitable for exploring the thermodynamic properties of QCD-like matter in both the confined and deconfined regimes [5,6].

In our earlier work [6], we mainly investigated this model through a dynamical observable, the Schwinger effect, while briefly examining a few thermodynamic quantities for comparison. Here we take the complementary approach of systematically analysing equilibrium thermodynamic probes of the phase structure within the same holographic background. Specifically, we study the behaviour of the heat capacity at fixed chemical potential and the number-density susceptibility χ_2. Our goal is to track how each of these quantities behaves across the first-order transition line, near the critical end point, and in the supercritical region. We observe that different probes exhibit distinct signatures and behaviours at transitions. We show that thermodynamic quantities such as the energy density, trace anomaly, and charge density are sensitive to first- and second-order phase transitions, but are unable to distinguish the crossover between confinement and deconfinement beyond the critical end point. In contrast, the heat capacity and the second-order susceptibility which are the first derivatives of the entropy and charge density, respectively, can signal the nature of the transition: they may exhibit a discontinuity at a first-order transition, a divergence at a second-order transition, and peaks whose sharpening depends on the proximity to the CEP. By following these features as functions of temperature and chemical potential, we identify how thermodynamic observables mark the crossover behaviour in the supercritical region. These results provide an additional perspective on the holographic study of QCD-like matter, presented in a compact and focused way.

Our presentation is structured as follows. In Section 2 we briefly review the holographic model and set our conventions, emphasising the version of the warp-factor used here. Section 3 introduces the thermodynamic ensemble, lists the relevant thermodynamic variables and defines the probes of interest, along with their expected qualitative behaviour in first-order, critical and crossover regimes. Subsections 3.1 and 3.2 present our numerical results. We close in Section 4 with a short summary and discussion.

2 The Holographic Model

To describe the strongly coupled plasma, we use the Einstein-Maxwell-Dilaton (EMD) setup, a five-dimensional gravitational theory capable of capturing both confinement and deconfinement features of QCD-like systems. The bulk dynamics are governed by

$$S = \frac{1}{16\pi G_5}\int d^5x\,\sqrt{-g}\left[R - \frac{1}{2}(\partial\phi)^2 - V(\phi) - \frac{1}{4}Z(\phi)F_{MN}F^{MN}\right], \tag{1}$$

where G_5 is the five-dimensional Newton constant, $V(\phi)$ is the dilaton potential, $Z(\phi)$ the gauge kinetic function, and F_{MN} the field strength tensor of a gauge field A_M.

The background fields take the ansatz

$$\begin{aligned} ds^2 &= e^{2A(z)}\left[-f(z)dt^2 + d\vec{x}^{\,2} + \frac{dz^2}{f(z)}\right], \\ A_M &= (A_t(z), 0, 0, 0, 0), \\ \phi &= \phi(z), \end{aligned} \tag{2}$$

with the AdS boundary at $z = 0$ and the horizon at $z = z_h$ where $f(z_h) = 0$. We have set the AdS radius to one, for simplicity.

The gauge kinetic function is taken to have the following simple form

$$Z(z) = e^{-cz^2 - A(z)}, \tag{3}$$

and the scale factor is chosen as

$$A(z) = -\frac{3}{4}\ln\left(az^2+1\right) + \frac{1}{2}\ln\left(bz^3+1\right) - \frac{3}{4}\ln\left(dz^4+1\right), \tag{4}$$

which reproduces a confining behaviour at low temperature while allowing black-hole solutions to exist throughout the temperature range. Unlike many other choices of scale factor, which lead to a thermal-AdS geometry representing the confining phase at low temperature, this form provides a unified metric ansatz in which both the confined and deconfined regimes can be described continuously, enabling a consistent thermodynamic analysis across the phase transition.

We use the parameter values found in Ref. [5]:

$$c = 1.16\ \text{GeV}^2, \quad a = 0.128889\ \text{GeV}^2, \quad b = 0.3625\ \text{GeV}^3, \quad d = 0.128889\ \text{GeV}^4. \tag{5}$$

The temporal component of the gauge field encodes the boundary chemical potential when expanded near the boundary position,

$$A_t(z) = \mu - \rho\, z^2 + \cdots, \tag{6}$$

where μ and ρ are the chemical potential and charge density, respectively. The regularity condition at the horizon requires $A_t(z_h) = 0$, which relates μ and ρ.

These boundary and regularity conditions ensure a well-defined configuration in the *grand-canonical ensemble*, where T and μ are control parameters.

The background solution is obtained through the *potential reconstruction method*, where the forms of $A(z)$ and $Z(\phi)$ are specified, and the dilaton potential $V(\phi)$ is reconstructed from the equations of motion [7–12]. This approach provides a self-consistent EMD solution suitable for thermodynamic analysis of the phase structure. The full details of solving the equations and the explicit forms of the functions $V(\phi)$, $A_t(z)$, $\phi(z)$ and $f(z)$ can be found in [5].

3 Thermodynamic Analysis

In this section we present the thermodynamic analysis of the holographic model introduced above. Our aim is to examine how the equilibrium quantities and their response functions reflect the phase structure of the dual QCD-like theory. We first compute the basic thermodynamic variables obtained from the black hole geometry, including temperature, quark number density, entropy density, pressure, energy density, trace anomaly, and the grand potential, and analyse their behaviour with respect to temperature and chemical potential. In particular, we show that the temperature and grand potential reveal the transition between the confining and deconfining branches of solutions, while the temperature dependence of the pressure, energy density, and trace anomaly agrees well with lattice QCD results. This discussion, presented in Subsection 3.1, sets the thermodynamic background for our later analysis. In Subsection 3.2, we turn to the thermodynamic response functions, such as the heat capacity and the susceptibility χ_2, which serve as sensitive probes of the different phases and the critical region of the model.

3.1 Deconfinement transition from basic thermodynamic quantities

In this subsection, starting from the background EMD solutions obtained in the previous section, we extract the physically charged black hole branches dual to nonconformal plasmas

by analysing their basic thermodynamic quantities: the temperature, entropy density, quark number density, and the grand canonical potential at fixed chemical potential.

The Hawking temperature is obtained from regularity of the Euclidean metric at the horizon radius z_h. Equivalently, it may be computed from the surface gravity κ. For the present metric ansatz one finds

$$T = \frac{\kappa}{2\pi} = -\frac{1}{4\pi}\,\partial_z f(z)|_{z=z_h} = \frac{1}{4\pi\left(1-e^{-cz_h^2}\right)^2}\frac{z_h^3\, e^{-3A(z_h)}}{\int_0^{z_h} dx\, x^3\, e^{-3A(x)}} \times \left[\left(1-e^{-cz_h^2}\right)^2 + 2c\mu^2\left(e^{-cz_h^2}\int_0^{z_h} dx\, x^3\, e^{-3A(x)} - \int_0^{z_h} dx\, x^3\, e^{-3A(x)} e^{-cx^2}\right)\right], \tag{7}$$

which relates the physical temperature to the slope of the blackening function at the horizon.

The entropy density follows from the Bekenstein–Hawking relation, evaluated on the horizon:

$$s = \frac{\mathcal{A}}{4G_5 V_3}\bigg|_{z=z_h} = \frac{e^{3A(z_h)}}{4G_5 z_h^3}, \tag{8}$$

where $\mathcal{A}$ is the transverse area and V_3 the spatial 3-volume. Both T and s are functions of z_h and the chemical potential μ.

In the grand canonical ensemble, the relevant thermodynamic potential is the grand potential density,

$$\Omega = \epsilon - Ts - \mu\rho, \tag{9}$$

where ϵ is the energy density and ρ is the quark number density. The first law at fixed spatial volume reads

$$d\Omega = -s\, dT - \rho\, d\mu, \tag{10}$$

which reduces to

$$d\Omega = -s\, dT, \tag{11}$$

when the chemical potential is held fixed. Integrating this relation, and imposing the standard holographic renormalization condition $\Omega(z_h \to \infty) = 0$, we obtain

$$\Omega(T,\mu) = \int_{z_h}^{\infty} s(z_h',\mu)\,\frac{\partial T}{\partial z_h'}\, dz_h'. \tag{12}$$

Once $T(z_h)$ and $\Omega(T)$ are determined for a given μ, the physically preferred branch for each boundary state (T,μ) is the one with the lowest value of the grand potential.

In Figure 1, we show $T(z_h)$ for several values of μ (left panel) and the corresponding grand potentials (right panel). For $\mu < \mu_{\rm cep}$, with $\mu_{\rm cep} \approx 312.192\,\text{MeV}$, the temperature curve exhibits three branches: a stable large black hole at small z_h, a stable small black hole at large z_h, and an intermediate unstable branch where T decreases with decreasing z_h. As μ increases, the unstable branch shrinks, and at $\mu = \mu_{\rm cep}$ the two stable branches merge at an inflection point. The three-branch structure in $T(z_h)$ manifests as a swallowtail in the grand potential (the right panel of Figure 1), which disappears for $\mu \geqslant \mu_{\rm cep}$. Such behaviour is characteristic of a first-order phase transition.

To illustrate the transition explicitly, Figure 2 displays $T(z_h)$ and $\Omega(T)$ at $\mu = 200\,\text{MeV}$ as an example of cases with $\mu < \mu_{\rm cep}$. The dashed region of the black hole solutions

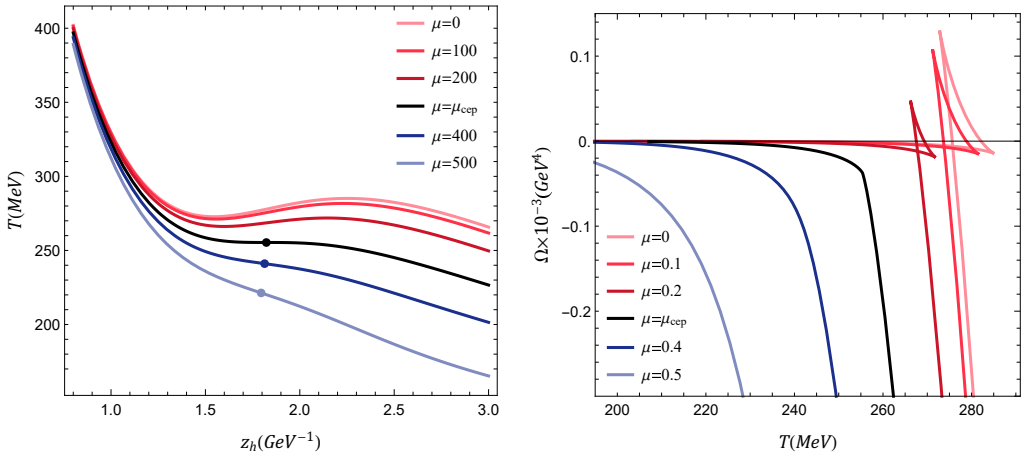

Figure 1: The left and right graphs show the temperature versus the horizon radius and the grand potential as a function of temperature for various values of the chemical potential, respectively.

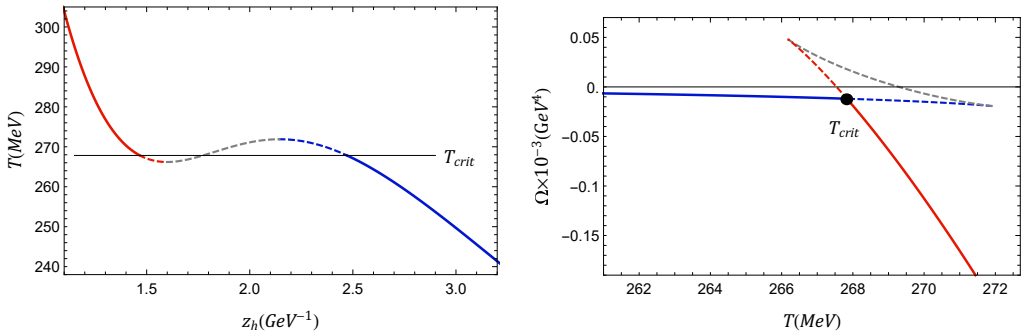

Figure 2: The temperature versus the horizon radius (left) and the grand canonical potential as a function of temperature (right), at $\mu = 200\,\mathrm{MeV}$. Dashed blue and red lines show the results for the metastable solutions, dashed gray lines represent the results for the nonphysial black hole solutions, and solid blue and red lines show the results for the ground state solutions at temperatures below and above transition temperature T_{crit}, respectively

contains two distinct parts. The first, presented by gray color, corresponds to the genuinely unstable branch, lying between the minimum and maximum of $T(z_h)$, where the temperature decreases as the black hole grows, i.e. as z_h decreases. These solutions are thermodynamically unstable and therefore unphysical. The second part, shown by dashed blue and red lines for large and small black holes respectively, consists of metastable solutions, which are physical in the sense that they satisfy all consistency conditions of the background but possess a higher grand potential than the blue and red stable branches as seen in the right panel of Figure 2. Consequently, although metastable configurations may exist at the same values of (T, μ), they are never energetically preferred in the grand canonical ensemble. From this figure and above discussion, we conclude that for sufficiently small μ there is a small/large black hole first-order transition, ending at the critical end point at μ_{cep}. In the dual gauge theory this corresponds to a first-order transition between the hadronic (confined) and quark-gluon plasma (deconfined) phases.

In what follows, we adopt the convention chosen for the graphs of Figure 2, for all thermodynamic plots: solid blue and red lines correspond to the energetically preferred solutions below and above the transition temperature $T_{\rm crit}$, respectively. These are those physical solutions with lowest Ω, corresponding respectively to the large and small stable black hole branches. The gray dashed lines denote the unstable nonphysical branch, and blue and red dashed curves represent, respectively, the metastable large and small black hole solutions.

From the grand potential we obtain the pressure density,

$$p = -\Omega, \tag{13}$$

and the energy density is determined through Eq. (9). Another important quantity is the trace anomaly, the trace of the energy–momentum tensor,

$$\Delta = \langle T^a{}_a \rangle = \epsilon - 3p, \tag{14}$$

which is nonzero due to the dilaton-induced breaking of conformal invariance.

To evaluate these quantities we also require the quark number density ρ. From the holographic dictionary,

$$A_t(z) = \mu - \rho\, z^2 + \cdots , \tag{15}$$

so reading off the coefficient of z^2 yields

$$\rho = \rho(\mu, z_h). \tag{16}$$

Figure 3 displays the pressure density, energy density, trace anomaly, and entropy density (each scaled by the required powers of temperature) as functions of temperature for various chemical potentials. At zero chemical potential, after the transition temperature, the scaled pressure, energy, and entropy density increase monotonically with T and approach constant values at large temperatures, in agreement with the Stefan–Boltzmann behaviour of non-Abelian plasmas. At nonzero finite chemical potential, all these quantities approach the same constants at large temperatures and independently of μ. The trace anomaly curves merge and approach zero at sufficiently high T, signalling restoration of approximate conformal symmetry. The enhancement of all observables with increasing μ contrasts with the behaviour reported in [13]. Notice that our zero-μ results are in qualitative agreement with lattice QCD data [14].

A further feature visible in these figures is the jump in the energy density, the trace anomaly and entropy density at $T_{\rm crit}$ for $\mu < \mu_{\rm cep}$, characteristic of a first-order transition. This is shown more clearly in Figs. 4 and 5, where we present enlarged plots for $\mu = 200\,\text{MeV}$ and $\mu_{\rm cep}$, containing the metastable and unstable solutions. Figure 4 shows the entropy density scaled by T^3 at $\mu = 200\,\text{MeV}$ and at the critical end point $\mu_{\rm cep}$. For chemical potentials below the CEP, the entropy exhibits a multivalued region near the transition temperature. In the left panel, we see that the entropy density increases with T for both the small and large black hole branches represented by the solid blue and red curves, as expected for physical configurations. It also grows with temperature along the metastable branches, shown by the blue and red dashed lines; these solutions are therefore physical but are not favored energetically compared with the solid-line branches. The gray dashed curve corresponds to the unstable branch, where the entropy decreases with temperature, confirming that these solutions are not physical. At $\mu = \mu_{\rm cep}$, the unstable and metastable branches disappear and the two physical branches merge. In this case, the entropy density increases monotonically with temperature for all remaining black hole solutions.

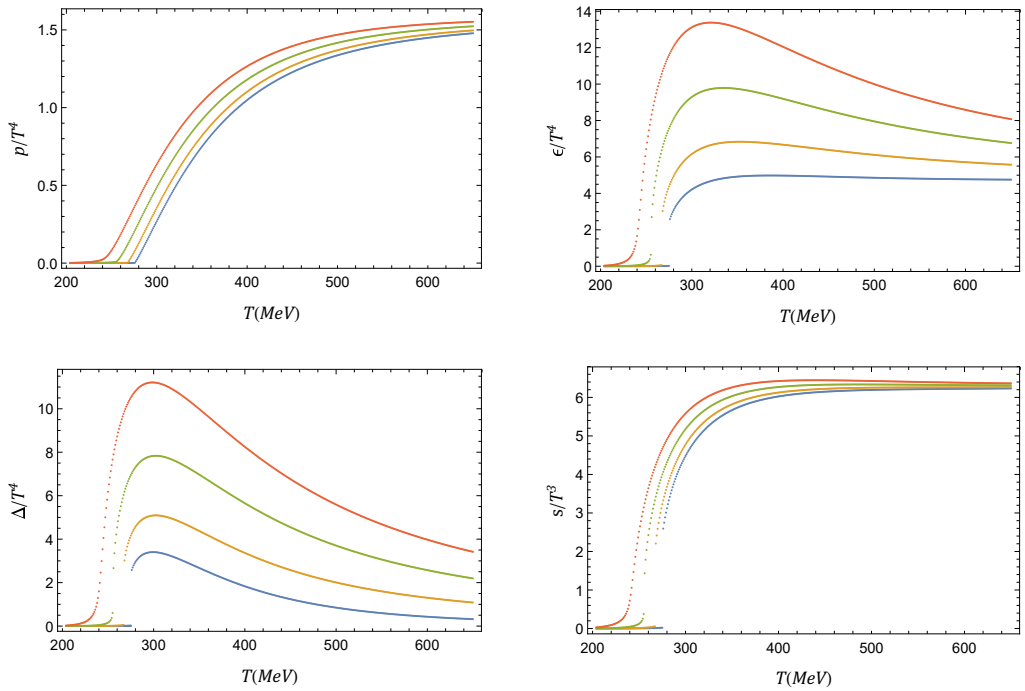

Figure 3: The temperature scaled pressure (top left), energy density (top right), trace anomaly (bottom left), and entropy density (bottom right). Chemical potential increases from blue to red (from bottom to top in each graph) and obtaines, respectively, the values $(0,\ 200,\ \mu_{\rm cep}, 400)$ in units MeV.

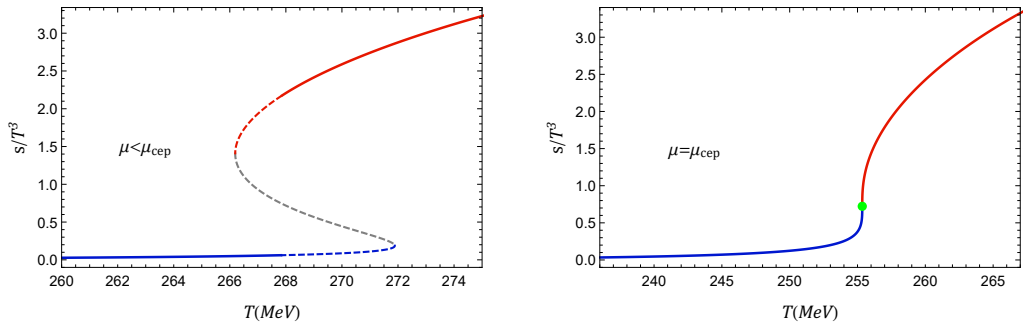

Figure 4: The entropy density for $\mu = 200\,\text{MeV}$ as an example of $\mu < \mu_{\rm cep}$ (left) and at $\mu_{\rm cep}$ (right). The line colors and styles follow the same convention described in Figure 2.

We depict the energy density and trace anomaly in Figure 5 to complete this discussion. The unstable and metastable solutions, shown by dashed curves, connect the two stable branches and are not thermodynamically preferred. At the critical end point, the stable branches merge and the other branches collapse to a point; consequently the jumps in the energy density and trace anomaly disappear, signalling a second-order transition. These observables therefore serve as reliable diagnostics for distinguishing first- and second-order behaviour. However, once the unstable branch disappears for $\mu > \mu_{\rm cep}$, these quantities vary smoothly and thus cannot be used to locate a putative crossover boundary between the

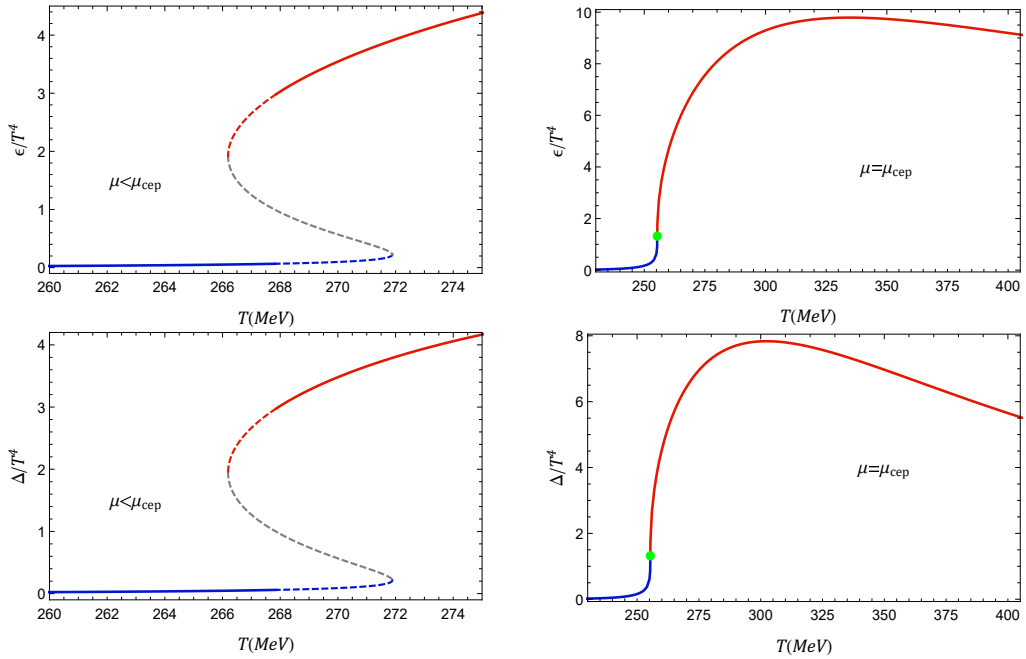

Figure 5: The scaled energy density (top) and trace anomaly (bottom) for a sample chemical potential below the CEP (left panels) and at $\mu_{\rm cep}$ (right panels). The line colors and styles follow the same convention described in Figure 2.

confined and deconfined phases in that region, as can be seen in Figure 3 for $\mu = 400\,\text{MeV}$ as an example of the supercritical region.

3.2 Thermodynamic response functions

In this subsection we examine the behavior of the thermodynamic response functions, namely the heat capacity at fixed chemical potential and the charge susceptibility, near the transition temperature. Since these quantities involve derivatives of the basic thermodynamic observables, they are particularly sensitive to critical behavior and therefore serve as reliable diagnostics of the phase structure.

The heat capacity at constant chemical potential and the charge susceptibility are defined as

$$C_\mu = -T\left(\frac{\partial^2\Omega}{\partial T^2}\right)_\mu = T\left(\frac{\partial s}{\partial T}\right)_\mu, \tag{17}$$

$$\chi = \left(\frac{\partial \rho}{\partial \mu}\right)_T. \tag{18}$$

Figure 6 displays the temperature dependence of the rescaled heat capacity for representative values of the chemical potential. For chemical potentials below the critical end point, as shown in the left panel, the heat capacity is positive for both the thermodynamically preferred solutions and the metastable ones, as expected for physical configurations. In contrast, it becomes negative for the unstable solutions (gray dashed lines), confirming their

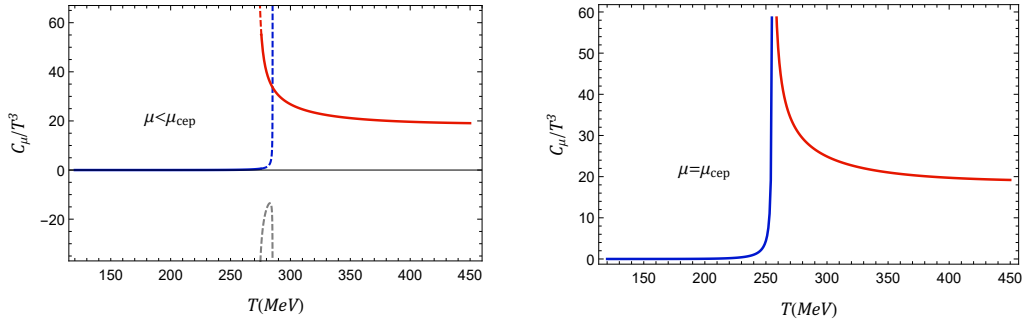

Figure 6: The temperature scaled heat capasity $\mu = 0$ (left) and μ_{cep} (right). The line colors and styles follow the same convention described in Figure 2.

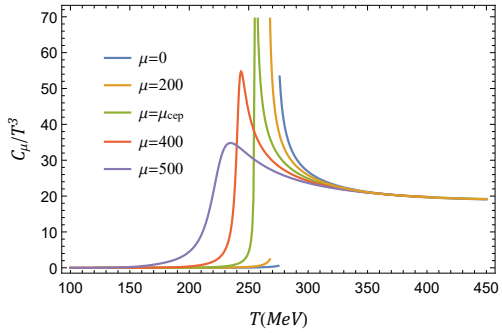

Figure 7: The temperature scaled heat capasity for various values of chemical potential.

thermodynamic instability. A finite discontinuity appears at the transition temperature due to the jump from the large black hole branch (solid blue line) to the small black hole branch (solid red line). This finite jump in C_μ, inherited from the discontinuity in the entropy, is the characteristic behavior of a first-order transition. At the critical end point, where only stable physical branches remain, this discontinuity is replaced by an infinite peak at the transition temperature, corresponding to the divergence of the heat capacity at T_{cep}.

The behavior changes qualitatively above the critical end point. As shown in Figure 7, the heat capacity develops a finite peak that gradually smoothens as the chemical potential increases. This continuous and nonsingular maximum is the typical signature of a crossover transition. In this figure we show only the heat capacity of the physical ground-state solutions.

The scaled charge density and charge susceptibility for various chemical potentials are depicted in Figs. 8 and 9. For a representative chemical potential below μ_{cep} (left panels of Figure 8), the charge density exhibits a multivalued structure, and its first derivative with respect to μ shows a finite discontinuity. This behavior is consistent with a first-order phase transition. Increasing the chemical potential to the critical value removes the multivalued region: the large and small black hole branches (solid blue and red curves) join at a single finite value of the charge density but with an infinite slope, leading to a divergence in the charge susceptibility at the critical temperature.

For $\mu > \mu_{cep}$, as seen in Figure 9, the charge density cannot be used to sharply distinguish the phases, since it varies smoothly across the transition region. Nevertheless, the charge susceptibility develops a finite maximum for any chemical potential above the critical end

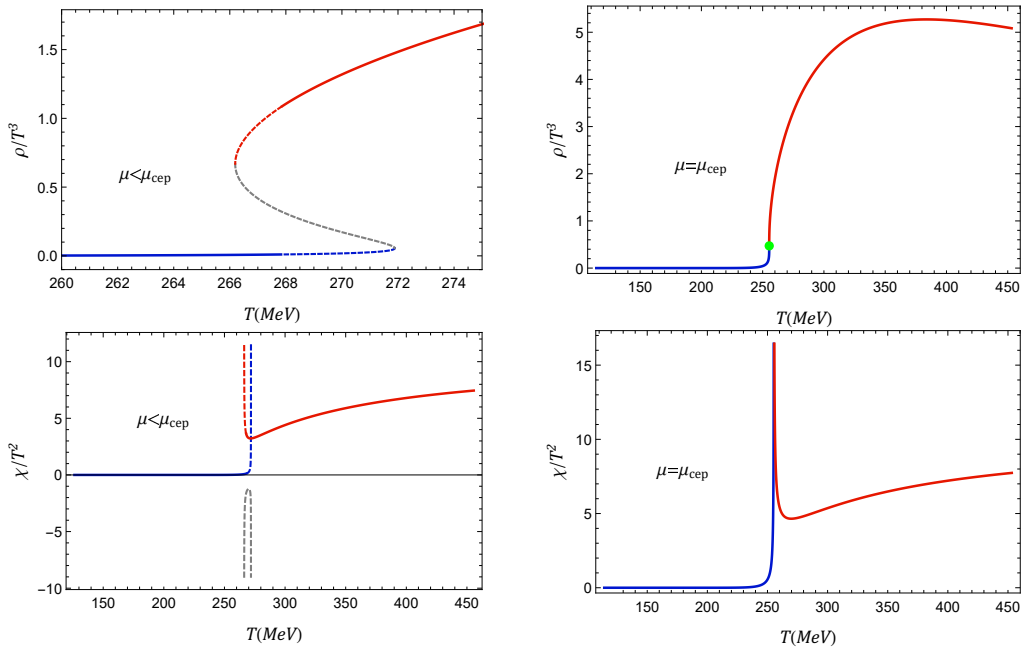

Figure 8: The rescaled charge density (top) and charge susceptibility (bottom) as functions of temperature for fixed values of the chemical potential; at $\mu = 200\,\mathrm{MeV}$ as an example of below the critical end point, $\mu < \mu_{\mathrm{cep}}$, (left) and at $\mu = \mu_{\mathrm{cep}}$ (right). The line colors and styles follow the same convention described in Figure 2.

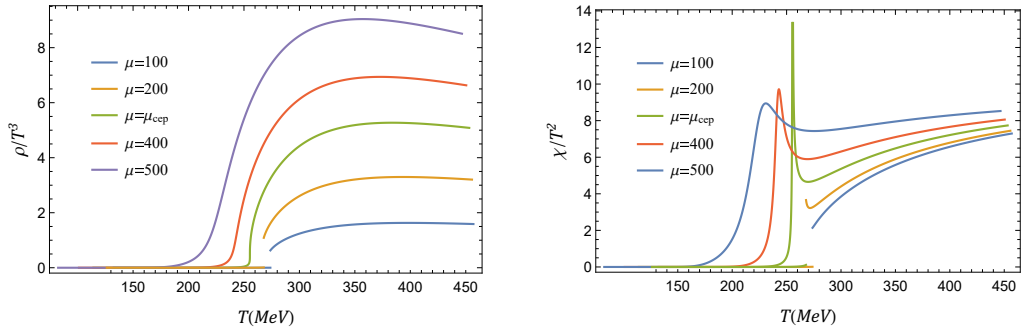

Figure 9: The rescaled charge density (left) and charge susceptibility (right) as functions of temperature for various values of the chemical potential.

point. This peak provides a clear indication of the crossover between the confined and deconfined regimes in this region of the phase diagram.

In summary, the heat capacity and the charge susceptibility offer sensitive probes of the thermodynamic phase structure. They correctly capture the first-order behavior below the critical end point, the divergence characteristic of the second-order critical point at μ_{cep}, and the smooth crossover behavior for $\mu > \mu_{\mathrm{cep}}$. Their behavior thus provides a coherent and physically consistent description of the different types of transitions present in the system.

4 Summary and concluding remarks

In this work, we have investigated the thermodynamics of an asymptotically AdS charged black hole solution in a holographic Einstein-Maxwell-dilaton (EMD) model describing a nonconformal plasma at finite temperature and chemical potential. Working in the grand canonical ensemble with fixed T and μ, we analyzed a range of thermodynamic quantities and response functions to characterize the equilibrium phases of the system. By employing a logarithmic form for the warp factor of the five-dimensional metric, capturing the dependence on temperature and chemical potential for both confined and deconfined phases, we obtained a set of black hole solutions exhibiting rich phase behavior, including first-order, second-order, and crossover transitions.

The thermodynamic structure obtained from the temperature, entropy density, grand potential, pressure, energy density, and trace anomaly displays the expected QCD-like pattern. At low chemical potentials, the multibranch behavior of $T(z_h)$ and the swallowtail form of the grand potential signal a first-order transition between small and large black holes. The unstable branch decreases with increasing μ and ends at a critical end point, beyond which all thermodynamic quantities vary smoothly, indicating a crossover. The pressure, energy density, entropy density, and trace anomaly behave consistently across the phase diagram and approach the Stefan-Boltzmann limit at high temperature, where their dependence on μ becomes negligible. The model shows qualitative agreement with lattice QCD at zero chemical potential.

Thermodynamic response functions provide further support. The heat capacity and charge susceptibility exhibit finite jumps at first–order transitions, diverge at the critical end point, and develop smooth maxima for $\mu > \mu_{\rm cep}$. While the charge density and entropy density alone cannot identify the crossover region, the susceptibility and heat capacity retain a characteristic peak that does. These features offer a unified picture of first-order, second-order, and crossover regimes.

In summary, the constructed model provides a coherent holographic framework for exploring equilibrium properties of strongly coupled systems with broken conformal symmetry and dynamical charge degrees of freedom at finite density. Future studies could investigate the transport coefficients, critical dynamics near the CEP, and real-time response functions in the crossover region. Another promising direction is the inclusion of scalar potentials fitted to lattice data at finite chemical potentials or coupling the model to additional bulk fields to capture flavor dynamics and chiral physics in a more realistic setting.

Data Availability

No data available.

Conflicts of Interest

The author declares that there is no conflict of interest.

Ethical Considerations

The author has diligently addressed ethical concerns, such as informed consent, plagiarism, data fabrication, misconduct, falsification, double publication, redundancy, submission, and other related matters.

Funding

This research did not receive any grant from funding agencies in the public, commercial, or non profit sectors.

References

[1] Gubser, S. S., Klebanov, I. R., & Polyakov, A. M. 1998, Phys. Lett. B 428, 105.

[2] Witten, E. 1998, Adv. Theor. Math. Phys., 2, 253.

[3] Maldacena, J. M. 1998, Adv. Theor. Math. Phys., 2, 231 [1999, Int. J. Theor. Phys., 38, 1113].

[4] Casalderrey-Solana, J., Liu, H., Mateos, D., Rajagopal, K., & U. Wiedemann, A. 2014, "Gauge/string duality, hot QCD and heavy ion collisions," Cambridge, UK: Cambridge University Press, 2014.

[5] Dudal, D. & Mahapatra, S. 2017, Phys. Rev. D, 96, 126010.

[6] Shahkarami, L. & Charmchi, F. 2026, JHEP, 02, 014. DOI: 10.1007/JHEP02(2026)014

[7] Alanen, J., Kajantie, K., & Suur-Uski, V. 2009, Phys. Rev. D, 80, 126008.

[8] Li, D., He, S., Huang, M., & Yan, Q. S., 2011, JHEP, 09, 041.

[9] He, S., Wu, S. Y., Yang, Y., & Yuan, P.-H. 2013, JHEP, 04, 093.

[10] Yang, Y. & Yuan, P.-H. 2015, JHEP, 12, 161.

[11] Aref'eva, I. & Rannu, K. 2018, JHEP, 05, 206.

[12] Bohra, H., Dudal, D., Hajilou, A., & Mahapatra, S. 2020, Phys. Lett. B, 801, 135184.

[13] Yang, Y. & Yuan, P-H. 2014, JHEP, 11, 149.

[14] Burger, F., Ilgenfritz, E.-M., Lombardo, M. P., & Muller-Preussker, M. 2015, Phys. Rev. D, 91, 074504.